

The *In situ* Electrochemical Detection of Microbubble Oscillations during Motion through a Channel

Peter R. Birkin^{a*}, Steven Linfield^a and Guy Denuault^a

^aDepartment of Chemistry, University of Southampton, Southampton, United Kingdom, SO17 1BJ

Figure S1 shows a still image of the experimental setup employed in the Coulter counting of microbubbles. The image shows the piston like emitter (PLE), the reflector (R), the glass microchannel (GMC), the cluster (C) and a surface bound bubble (SB) on the body of the GMC.

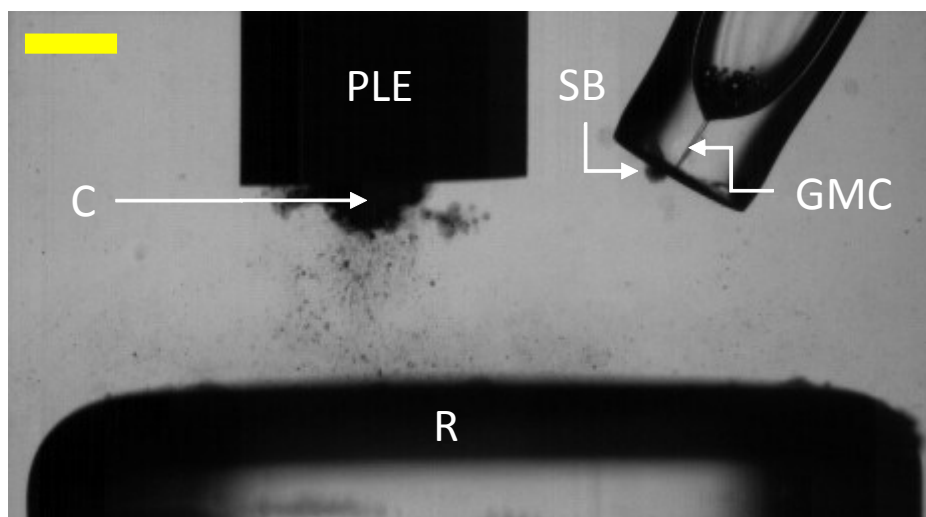


Figure S1. Image of the experimental setup deployed in the experiments. The PLE was 2.5 ± 0.1 mm from the surface of the reflector (R). The GMC edge was 1 ± 0.1 mm from the PLE. This meant the $40 \mu\text{m}$ channel was ~ 3.2 mm laterally away from the center of the PLE where the cluster (C) can be seen. A surface bubble (SB) on the outside of the capillary used to make the GMC is also highlighted. The scale bar represents 1 mm.

Movie S1 shows the bubble activity imaged at 20 kfps under these conditions. This shows a sequence of translocation events, with a small single bubble translocating near the start, followed by the surface bubble (SB) observed later in the sequence. Some fragmentation can be seen during the translocation of the surface bubble (SB).

Figure S2 shows a sequence with three different translocation events. These are labelled (a), (b) and (c)

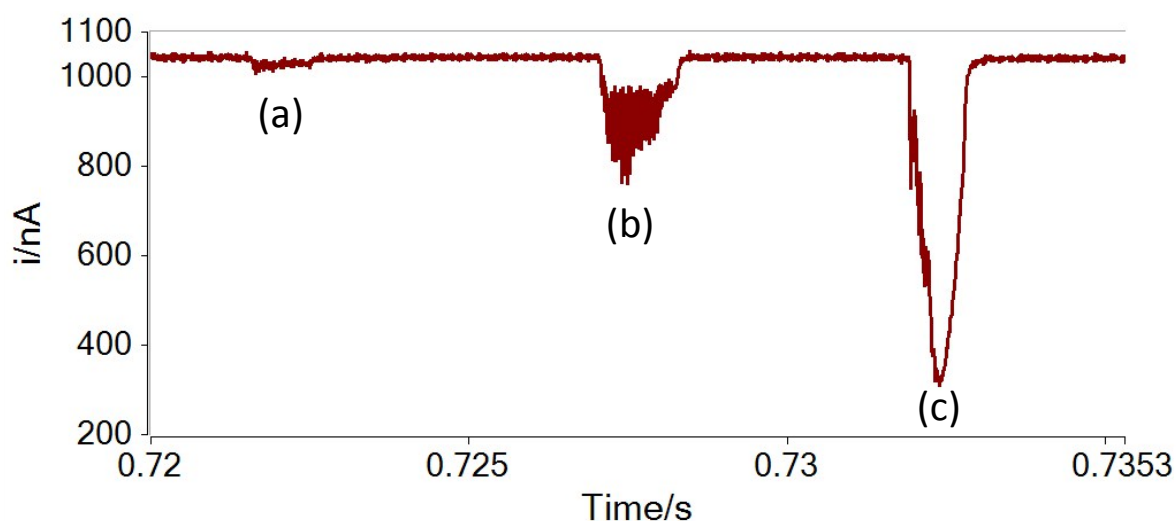


Figure S2. Plot showing the ion current (i , —) as a function of time for a 40 μm diameter pore. The GMC was positioned ~ 3 mm laterally and level with the PLE which was operated at $2 W_{\text{rms}}$. The aerobic solution contained 10 mM KCl. A potential of 5 V was applied across the pore. A pressure difference of 72 mBar was applied to draw liquid into the GMC. The solution temperature was ~ 25 $^{\circ}\text{C}$. The annotation (a), (b) and (c) refers to three translocation events of different bubble size.

Event (a) is the smallest and can only just be detected above the baseline (with respect to the noise). Event (b) is larger and shows clear oscillations during the translocation. Event (c) is the largest in this sequence, but shows less evidence of bubble oscillation. Each of these three events were imaged using a high-speed camera, as seen in Movie S2. This shows that event (a) is likely to be a single bubble, (b) is actually two bubbles translocating at the same time, while (c) is a large surface bubble that translocates as a ‘slug’ and leaves a smaller surface bubble behind. The data suggests that the ‘slugs’ oscillate less as they translocate, presumably as a result of their geometry and that of the channel in the GMC. In addition to the Movies S2, a composite showing the imaging and the current time history (with a moving cursor) is available as Movie S3. Although this links the two sets of data, the imaging of the bubble translocation is limited by resolution issues in this case. This means that sizing directly from the imaging is not possible. However, the ionic current perturbation of translocation can be used to make an estimate of the bubble size (see main text).

Figure S3 shows the frequency components present in the hydrophone data acquired for the PLE operating at a reported power of $2 W_{\text{rms}}$. This shows one distinct frequency at the fundamental of the ultrasonic source (22-23 kHz) with little subharmonic emission. This agrees with the data acquired for the current time events under these conditions. However, note that the current time data only contains significant signals at the PLE frequency (f) during bubble translocation. This indicates that these component are due to bubble oscillation during translocation and are not due to noise pickup (see main paper).

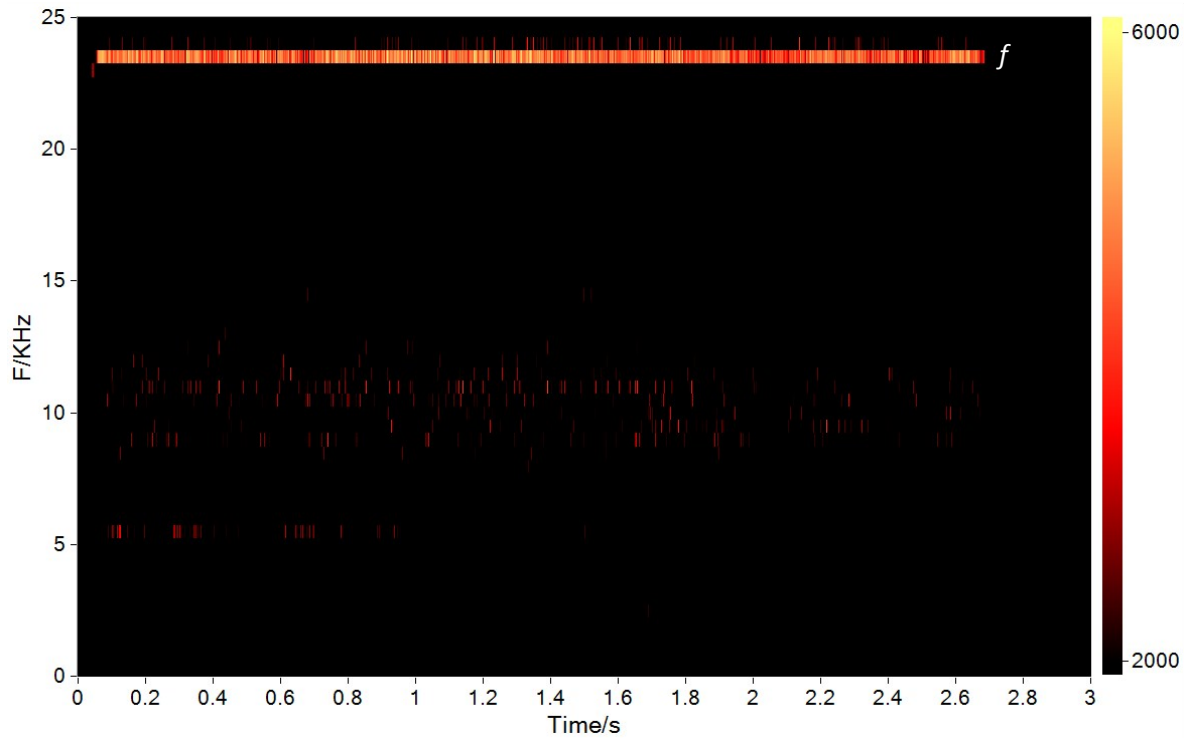


Figure S3 Plots showing the frequency components as a function of time detected by a hydrophone placed in the solution ~ 10 - 15 mm laterally from the PLE. The PLE was operated at $2 W_{\text{rms}}$. The aerobic solution contained 10 mM KCl. The solution temperature was ~ 28 $^{\circ}\text{C}$. The scale bar represents acoustic pressure in Pa. Note the fundamental frequency of the PLE (~ 23 kHz) is shown with the annotation ' f '.

Figure S4 shows the frequency components present in the hydrophone data acquired for the PLE operating at a reported power of $18 W_{\text{rms}}$. This shows one distinct frequency at the fundamental of the ultrasonic source (22 - 23 kHz, f) with two detectable subharmonic emission¹ (at $2f/3$ and $f/3$). This agrees with the data acquired for the current time events under these conditions.

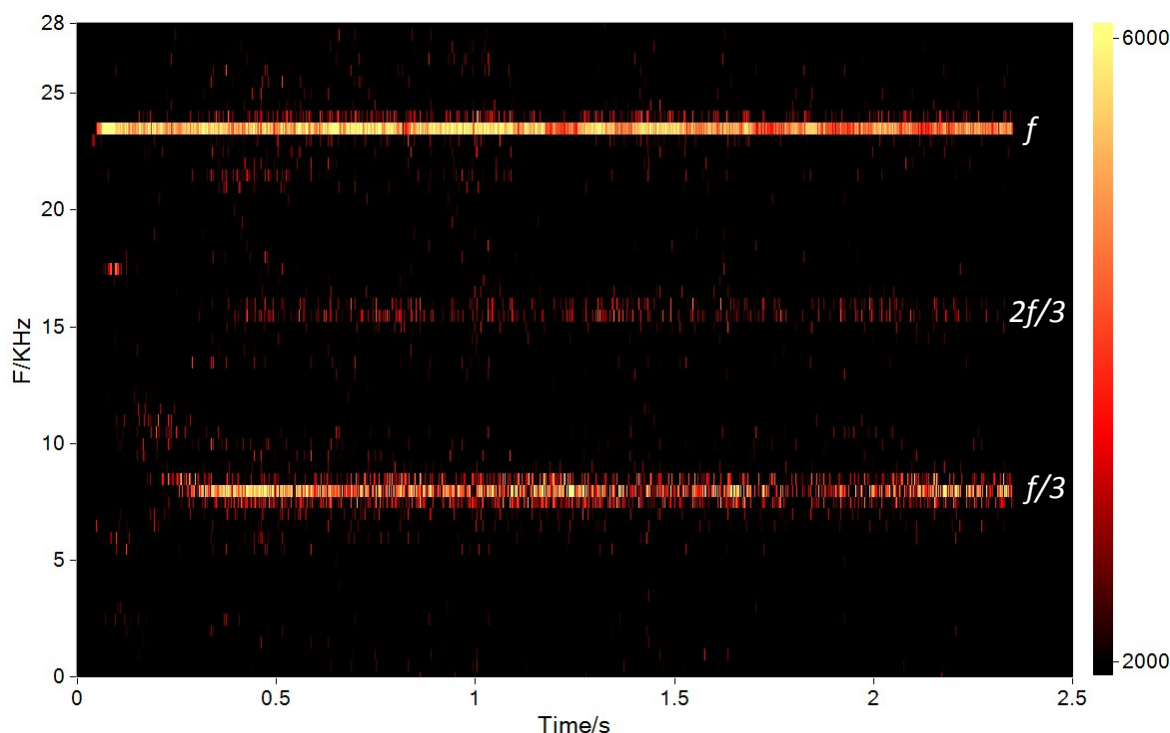


Figure S4. Plots showing the frequency components as a function of time detected by a hydrophone placed in the solution $\sim 10\text{-}15$ mm laterally from the PLE. The PLE was operated at a power of $18 W_{\text{rms}}$. The aerobic solution contained 10 mM KCl. The solution temperature was ~ 28 °C. The scale bar represents acoustic pressure in Pa. Note the fundamental frequency of the PLE (~ 23 kHz) is shown with the annotation ' f '. Subharmonics in the data are annotated with ' $2f/3$ ' and ' $f/3$ '.

To calculate the size of the bubbles that translocate in the main paper (see figure 4), the following approach was adopted. First, the current time data was analysed using a DSP(FFT) approach and the 0 Hz (or DC) component extracted (see figure 4 (a)). This represents the time average signal of the current over the 2 ms time window considered. Second, this current was converted to an effective resistance change and combined with standard Coulter counter theory. Equation (1) shows the relevant formula

$$\Delta R = \left(\frac{4\kappa d^3}{\pi D^4} \right) f \quad (1).$$

where ΔR is the change in resistance, κ the electrolyte conductivity², d the bubble diameter, D the pore diameter and f a correction factor based on the published data by Smythe³⁻⁵. This approach has been used with similar pores and monodispersed polystyrene spheres and shown to be accurate⁶.

References

- 1 P. R. Birkin, T. M. Foley, T. T. Truscott, A. Merritt and S. Martini, Cavitation clusters in lipid systems – surface effects, local heating, outgassing and streamer formation, *Phys. Chem. Chem. Phys.*, 2017, **19**, 6785–6791.
- 2 R. B. McCleskey, Electrical Conductivity of Electrolytes Found In Natural Waters from (5 to 90)

- °C, *J. Chem. Eng. Data*, 2011, **56**, 317–327.
- 3 J. L. Anderson and J. A. Quinn, The relationship between particle size and signal in coulter-type counters, *Rev. Sci. Instrum.*, 1971, **42**, 1257–1258.
 - 4 W. R. Smythe, Flow around a spheroid in a circular tube, *Phys. Fluids*, 1964, **7**, 633–638.
 - 5 W. R. Smythe, Flow around a sphere in a circular tube, *Phys. Fluids*, 1961, **4**, 756–759.
 - 6 P. R. Birkin, S. Linfield, G. Denuault, R. Jones, J. Youngs and E. Wain, An analytical differential resistance pulse system relying on a time shift signal analysis – applications in Coulter counting, *ACS Sensors*, 2019, **4**, 2190–2195.